JOURNAL OF AGRICULTURAL AND FOOD CHEMISTRY

Article

pubs.acs.org/JAFC

Epicatechin Gallate Impairs Colon Cancer Cell Metabolic Productivity

Susana Sánchez-Tena,[†,‡] Gema Alcarraz-Vizán,[†,‡,⊥] Silvia Marín,[†,‡] Josep Lluís Torres,[§] and Marta Cascante*[,†,‡]

[†]Department of Biochemistry and Molecular Biology, Faculty of Biology, Universitat de Barcelona, Avinguda Diagonal 643, 08028 Barcelona, Spain

[‡]Institut de Biomedicina de la Universitat de Barcelona (IBUB) and Unit Associated with CSIC, Avinguda Diagonal 643, 08028 Barcelona, Spain

[§]Department of Biological Chemistry and Molecular Modelling, Institute for Advanced Chemistry of Catalonia, IQAC-CSIC, Jordi Girona 18-26, 08034 Barcelona, Spain

ABSTRACT: Green tea and grape phenolics inhibit cancer growth and modulate cellular metabolism. Targeting the tumor metabolic profile is a novel therapeutic approach to inhibit cancer cell proliferation. Therefore, we treated human colon adenocarcinoma HT29 cells with the phenolic compound epicatechin gallate (ECG), one of the main catechins in green tea and the most important catechin in grape extracts, and evaluated its antiproliferation effects. ECG reduced tumor viability and induced apoptosis, necrosis, and S phase arrest in HT29 cells. Later, biochemical determinations combined with mass isotopomer distribution analysis using [1,2-$^{13}C_2$]-D-glucose as a tracer were used to characterize the metabolic network of HT29 cells in response to different concentrations of ECG. Glucose consumption was importantly decreased after ECG treatment. Moreover, metabolization of [1,2-$^{13}C_2$]-D-glucose indicated that the *de novo* synthesis of fatty acids and the pentose phosphate pathway were reduced in ECG-treated cells. Interestingly, ECG inhibited the activity of transketolase and glucose-6-phosphate dehydrogenase, the key enzymes of the pentose phosphate pathway. Our data point to ECG as a promising chemotherapeutic agent for the treatment of colon cancer.

KEYWORDS: *ECG, grape, tea, metabolism, colon cancer*

INTRODUCTION

Colorectal cancer is one of the most prevalent causes of cancer-related mortality in the Western world.[1] Therefore, further development of therapeutic and preventive means of controlling this disease is clearly needed. Epidemiological and experimental studies have linked a diet rich in fruits, vegetables, and beverages containing polyphenolic compounds to the prevention of colon cancer, among other diseases. In particular, epicatechin gallate (ECG), one of the major catechins in green tea and grape, has been described as a potent protector against colorectal cancer in a cell-type-dependent manner. ECG induced apoptosis in SW480 cells through ERK activation, AKT inhibition, imbalance among anti- and pro-apoptotic protein levels, and caspase-3 activation. However, in Caco2 cells, ECG only increased the antioxidant potential without affecting cell growth.[2] Another study showed that ECG induces G1 phase cell cycle arrest and apoptosis in HCT116 colon cancer cells.[3] Moreover, recent *in vitro* and *in vivo* studies have suggested that green tea and grape polyphenols have preventive effects against the development of metabolic diseases such as obesity, insulin resistance, hypertension, and hypercholesterolemia.[4,5]

Multiple lines of evidence show that tumorigenesis is often associated with a metabolic adaptation characterized by, among others, the broadly known Warburg effect (increased fermentation of glucose to lactate even in the presence of oxygen), the activation of biosynthetic pathways, and the overexpression of some isoenzymes. These robust characteristics confer a common advantage to different types of cancers by increasing the ability of cells to survive, proliferate, and invade.[6] Therefore, a better knowledge of the tumor metabolic profile required to support proliferation is necessary for the development of novel therapeutic strategies against cancer. By studying how antiproliferative natural products alter this metabolic profile in cancer-derived cell lines, we are revealing potential targets for therapeutic strategies against cancer.

Stable isotope tracing, using [1,2-$^{13}C_2$]-D-glucose as a source of carbon in combination with mass spectrometry to detect substrate flow and specific distribution patterns of ^{13}C isotopomers, allows the evaluation of metabolic fluxes through the main pathways that facilitate energy production and biosynthetic metabolism. Examples of the strength of this approach include the characterization of the metabolic adaptation underlying angiogenic activation[7] and the elucidation of distinctive metabolic phenotypes that correlate with different codon-specific mutations in *K-ras* in NIH3T3 mice fibroblasts.[8]

In the present study, we use this powerful methodology to gain insight into the targeting of the tumor metabolic profile of human colon adenocarcinoma HT29 cells by ECG.

Received: December 10, 2012
Revised: April 3, 2013
Accepted: April 17, 2013
Published: April 17, 2013

dx.doi.org/10.1021/jf3052785 | *J. Agric. Food Chem.* 2013, 61, 4310−4317

MATERIALS AND METHODS

Chemicals. All chemicals were purchased from Sigma-Aldrich Co. (St Louis, MO, USA), unless otherwise specified. Dulbecco's modified Eagle's medium (DMEM) and antibiotic (10 000 U/mL penicillin, 10 000 μg/mL streptomycin) were obtained from Gibco-BRL (Eggenstein, Germany). Fetal calf serum (FCS) and trypsin−EDTA solution C (0.05% trypsin−0.02% EDTA) were from Invitrogen (Paisley, UK). Stable [1,2-$^{13}C_2$]-D-glucose isotope was obtained with >99% purity and 99% isotope enrichment for each position from Isotec Inc. (Miamisburg, OH, USA).

Cell Culture. Human colorectal adenocarcinoma HT29 cells (obtained from the American Type Culture Collection, HTB-38) were grown as a monolayer culture in DMEM (with 4 mM L-glutamine, without glucose, and without sodium pyruvate) in the presence of 10% heat-inactivated fetal calf serum, 10 mM glucose, and 0.1% streptomycin/penicillin in standard culture conditions. Cells were cultured at 37 °C in 95% air, 5% CO_2 humidified environment. HT29 cell cultures were started with 3×10^5 cells in 60 cm^2 Petri dishes as determined by using standard cell-counting techniques. Twenty-four hours after seeding, the culture medium was removed and replaced with fresh medium supplemented with [1,2-$^{13}C_2$]-D-glucose (50% isotope enrichment) with 70 μM ECG, 140 μM ECG, or without ECG. The cells were harvested 72 h after treatment.

Determination of Cell Viability. Cell viability was assessed using a variation of the MTT assay.[9] The assay is based upon the principle of reduction of MTT into blue formazan pigments by viable mitochondria in healthy cells. HT29 cells were seeded at a density of 3×10^3 cells/well in 96-well flat-bottom plates. After 24 h of incubation at 37 °C, ECG was added to the cells at different concentrations in fresh medium. The culture was incubated for 72 h. Next, the medium was removed, and 50 μL of MTT (1 mg/mL in PBS) with 50 μL of fresh medium was added to each well and incubated for 1 h. The MTT was reduced to a blue formazan product, and the precipitate was dissolved in 100 μL of DMSO. Absorbance values were measured on an ELISA plate reader (550 nM) (Tecan Sunrise MR20-301, Tecan, Salzburg, Austria). Absorbance was taken as proportional to the number of living cells.

Cell Cycle Analysis by FACS. The cell cycle was analyzed by measurement of the cellular DNA content using the fluorescent nucleic acid dye propidium iodide (PI) to identify the proportion of cells that are in each stage of the cell cycle. The assay was carried out using flow cytometry with a fluorescence-activated cell sorter (FACS). HT29 cells were plated in six-well flat-bottom plates at a density of 87×10^3 cells/well. After 24 h of incubation at 37 °C, ECG was added to the cells at 70 and 140 μM. After 72 h of incubation, cells were trypsinized, pelleted by centrifugation (400g for 5 min), and stained in Tris-buffered saline (TBS) containing 50 μg/mL PI, 10 μg/mL RNase free of DNase, and 0.1% Igepal CA-630. They were incubated in the dark for 1 h at 4 °C. Cell cycle analysis was performed by FACS (Epics XL flow cytometer, Coulter Corp., Hialeah, FL, USA) at 488 nm.

Apoptosis Analysis by FACS. Double staining with annexin V-FITC and propidium iodide was used to determine the percentage of apoptotic cells. At the start of apoptosis phosphatidylserine (PS) translocates from the inner to the outer membrane, thereby exposing phosphatidylserine to the external environment.[10] The phospholipid-binding protein annexin V, which is flourescently labeled with FITC (fluourescein isothiocyanate), has a high affinity for phosphatidylserine, so it binds to early apoptotic cells. Additionally, we can also quantify PI-permeable cells due to processes such as necrosis, which affect the integrity of the cell membrane. Annexin+/ PI− cells were then considered early apoptotic cells. Moreover, annexin+/PI+ and annexin−/PI+ cells were represented together as late apoptotic/necrotic cells, since this method does not differentiate necrotic cells from cells in late stages of apoptosis, which are also permeable to PI. Annexin V-FITC and PI staining were measured by FACS. Cells were seeded, treated, and collected as described in the previous section. After centrifugation (400g for 5 min), cells were washed in binding buffer (10 mM Hepes, pH 7.4, 140 mM sodium chloride, 2.5 mM calcium chloride) and resuspended in the same buffer. Annexin V-FITC was added using the annexin V-FITC kit. Afterward, cells were incubated for 30 min at room temperature in the dark. Next, propidium iodide was added 1 min before the FACS analysis at 20 μg/mL. Flourescence was measured at 495 nm (annexin V-FITC) and 488 nm (PI).

Glucose, Lactate, and Glutamine Concentration. The glucose, lactate, and glutamine concentrations in the culture medium were measured spectrophotometrically using a Cobas Mira Plus chemistry analyzer (Horiba ABX, Montpellier, France) at the beginning and at the end of the incubation period, to calculate glucose/glutamine consumption and lactate production.

Lactate Mass Isotopomer Analysis. To measure lactate by gas chromatography coupled to mass spectrometry (GC/MS), this metabolite was extracted by ethyl acetate after acidification with HCl and derivatized to its propylamideheptafluorobutyric form.[11] The m/z 328 (carbons 1−3 of lactate, chemical ionization) was monitored for the detection of m0 (unlabeled species), m1 (lactate with one ^{13}C atom), and m2 (lactate with two ^{13}C atoms).

Glutamate Mass Isotopomer Analysis. Glutamate was separated from the cell medium using ion-exchange chromatography as described elsewhere.[12] Glutamate was converted to its n-trifluoroacetyl-n-butyl derivative, and the ion clusters m/z 198 (carbons 2−5 of glutamate, electron impact ionization) and m/z 152 (carbons 2−4 of glutamate, electron impact ionization) were monitored.

Fatty Acid Mass Isotopomer Analysis. Fatty acids were extracted by saponification of the Trizol (Invitrogen, Carlsbad, CA, USA) cell extract after removal of the RNA-containing supernatant. Cell debris was treated with 30% KOH and 100% ethanol overnight, and the extraction was performed using petroleum ether.[11] Fatty acids were converted to its methyl ester derivative, and the ion clusters m/z 269 (palmitate (C16), electronic impact ionization) and m/z 297 (stearate (C18), electronic impact ionization) were monitored.

RNA Ribose Mass Isotopomer Analysis. RNA ribose was isolated by acid hydrolysis of cellular RNA after Trizol purification of cell extracts. Ribose isolated from RNA was derivatized to its aldonitrile acetate form using hydroxylamine in pyridine and acetic anhydride.[11] The ion cluster around m/z 256 (carbons 1−5 of ribose, chemical ionization) was monitored.

Gas Chromatography/Mass Spectrometry. Mass spectral data were obtained on a GCMS-QP2010 selective detector connected to a GC-2010 gas chromatograph from Shimadzu. The settings were as follows: GC inlet 200 °C, transfer line 280 °C, MS Quad 150 °C. A HP-5MS capillary column (30 m length, 250 μm diameter, and 0.25 μm film thickness) was used for the analysis of lactate, glutamate, and ribose. On the other hand, for the analysis of fatty acids, the GC inlet was set at 250 °C, and a bpx70 (SGE) column (30 m length, 250 μm diameter, and 0.25 μm film thickness) was used.

Activity of the Pentose Phosphate Pathway Enzymes Glucose-6-phosphate Dehydrogenase (G6PD) and Transketolase (TKT). Cell cultures were washed with PBS and scrapped in lysis buffer (20 mM Tris-HCl, pH 7.5, 1 mM dithiothreitol, 1 mM EDTA, 0.02% Triton X-100, 0.02% sodium deoxycholate). Cells were homogenized on ice-cold buffer following three cycles of 10 s of sonication with a titanium probe and immediately centrifuged at 13000g for 20 min at 4 °C. The supernatant was used for the determination of enzyme activities by adapting a previously described method[13] to a Cobas Mira Plus chemistry analyzer. Briefly, G6PD (EC 1.1.1.49) activity was evaluated by measuring the absorbance changes at 340 nm as a result of NADPH formation recorded for 15 min after the addition of 10 μL of sample to a cuvette containing 0.5 mM $NADP^+$ in 50 mM Tris-HCl, pH 7.6, at 37 °C. Reactions were initiated by the addition of G6P up to a final concentration of 2 mM. The method for TKT (EC 2.2.1.1) analysis is based on its product, glyceraldehyde-3-phosphate, which is isomerized to dihydroxyacetone-phosphate, and in turn, its conversion to glycerol-phosphate consumes NADH, which absorbs at 340 nm. Briefly, samples were added to a cuvette containing 5 mM $MgCl_2$, 0.2 U/mL triose phosphate isomerase, 0.2 mM NADH, and 0.1 mM thiamine pyrophosphate in 50 mM Tris-HCl, at pH 7.6 and 37 °C. The reaction was initiated by the addition of a substrate mixture in 1:2 proportion (substrate

mixture:final volume) prepared by dissolving 50 mM R5P in 50 mM Tris-HCl, pH 7.6, with 0.1 U/mL ribulose-5-phosphate-3-epimerase and 1.7 mU/mL phosphoriboisomerase. Protein concentration of cell extracts was determined using the BCA Protein Assay (Pierce Biotechnology, Rockford, IL, USA). Enzyme activities are expressed as mU/mg protein.

Data Analysis and Statistical Methods. *In vitro* experiments were carried out using three cultures each time for each treatment. Mass spectral analyses were carried out by three independent automatic injections of 1 μL of each sample by the automatic sampler. Statistical analyses were performed using one-way ANOVA followed by the Bonferroni multiple-comparison test.

RESULTS

Inhibition of HT29 Cell Proliferation by ECG. HT29 cells were treated with different doses of ECG, and cell proliferation was assessed. Figure 1A shows the dose−viability curve from which ECG concentrations used for further experiments were selected. A nontoxic but still active concentration of ECG, 70 μM ECG dose, which produced an 18 ± 4% reduction in proliferation, was selected and also a higher concentration of 140 μM, which caused a more significant reduction in HT29 cell proliferation of 70 ± 11%. Later, HT29 cell number was determined after treatment with 70 and 140 μM ECG for 24, 48, and 72 h (Figure 1B). Both ECG concentrations decreased the rate of cell growth compared to control HT29 cells.

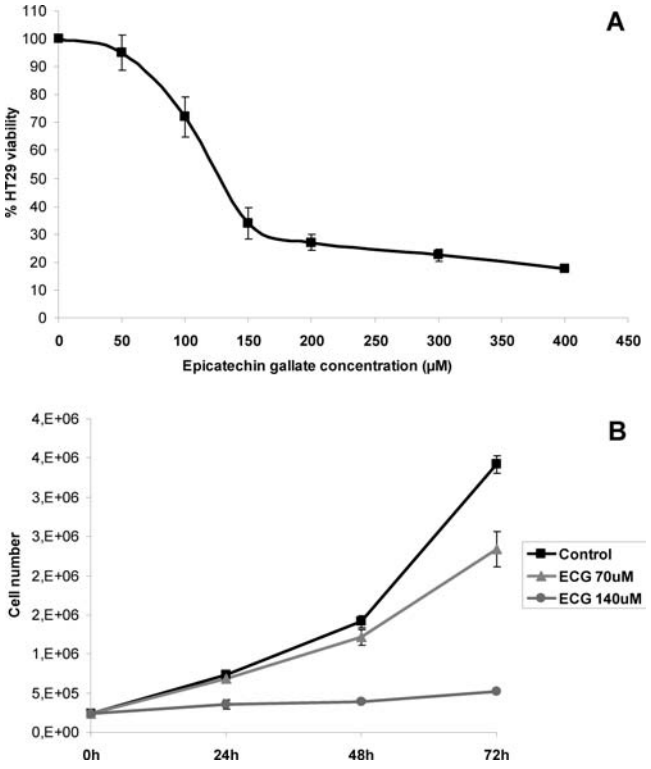

Figure 1. (A) Effect of increasing concentrations of ECG on HT29 cell proliferation. Values are expressed as means of the percentage of cell viability with respect to control cells ± standard deviation (SD), N = 3. (B) Number of cells over time. Mean ± SD, N = 3.

Cell Cycle and Apoptosis in HT29 Colon Adenocarcinoma Cells. To further investigate the mechanism by which ECG treatment affects cell proliferation, we analyzed the cell cycle and apoptosis by flow cytometry after treatment with 70 and 140 μM ECG for 72 h. As shown by staining with propidium iodide, only HT29 cells treated with 140 μM ECG showed a significant increase in the population in the S phase (Figure 2A). Regarding apoptosis analysis, 70 μM ECG produced a slight but not significant increase in apoptosis and necrosis (Figure 2B). However, 140 μM ECG induced significant percentages of both apoptosis and necrosis in HT29 cells (Figure 2B).

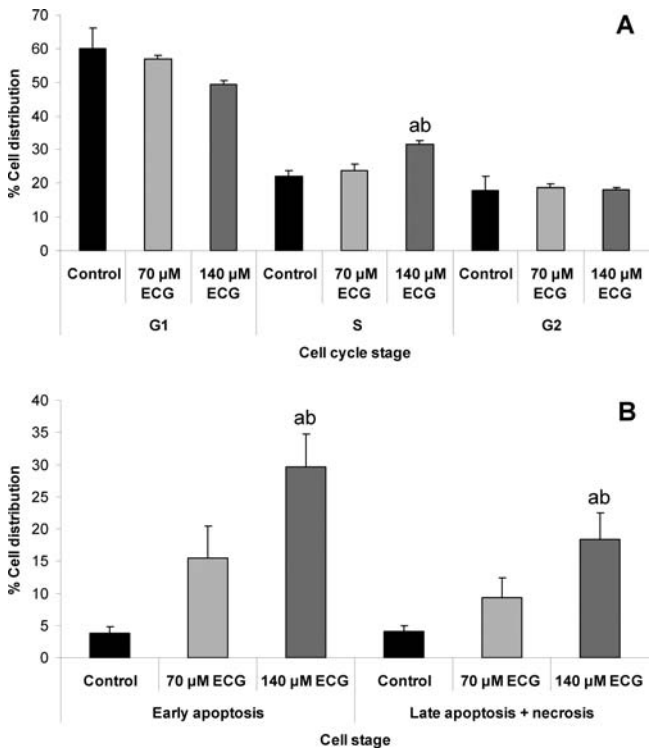

Figure 2. (A) Cell cycle analysis by flow cytometry after treatment with ECG for 72 h. Cell phases analyzed: G1, S, and G2. Mean ± SD, N = 3. (B) Flow cytometry analysis of double staining with annexin V-FITC and PI after exposure of HT29 cells to ECG for 72 h. Early apoptotic cells: annexin V+PI−; late apoptotic/necrotic cells: annexin V+/PI+ and annexin V−/PI+. Values are expressed as mean ± SD, N = 3. Significant differences are identified with different letters ($p < 0.05$ by one-way ANOVA following Bonferroni test): [a]Significantly different from control; [b]Significantly different from 70 μM ECG.

Glucose and Glutamine Consumption and Lactate Production in ECG-Treated HT29 Cells. Glucose and glutamine consumption and lactate production were estimated in HT29 cells before and after 72 h of ECG treatment and normalized by the amount of cells present during that time (area under the curve in Figure 1B). Figure 3 shows the values for normalized glucose consumption (A), lactate production (B), and glutamine consumption (C) in ECG-treated and nontreated (control) cells. Treatment with 70 μM ECG did not affect glucose and glutamine consumption and lactate production. However, treatment with 140 μM ECG significantly reduced glucose consumption by 77% and increased glutamine consumption by 48%.

Lactate Mass Isotopomer Distribution Was Not Significantly Affected by ECG. The lactate mass isotopomer distribution can be used to calculate the total lactate enrichment measured as $\sum mn = m1 + m2 \times 2$. This parameter represents the average number of ^{13}C atoms per molecule and indicates the *de novo* synthesis from labeled glucose. The

dx.doi.org/10.1021/jf3052785 | J. Agric. Food Chem. 2013, 61, 4310−4317

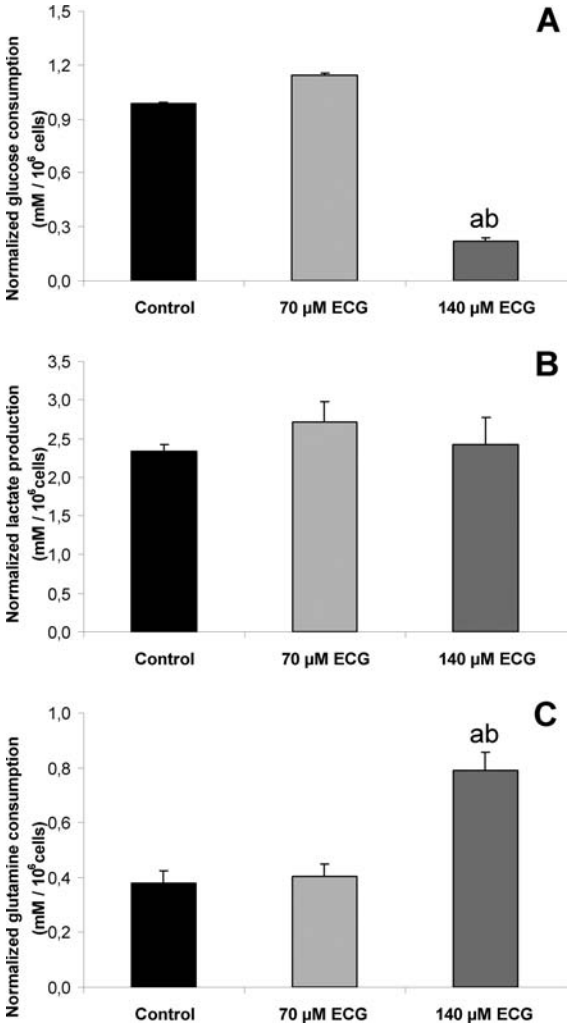

Figure 3. Effect of ECG on glucose (A) and glutamine (C) consumption and on lactate production (B). Mean ± SD, $N = 3$. $p < 0.05$ by ANOVA test followed by Bonferroni correction: [a]Significantly different from the control; [b]Significantly different from 70 μM ECG.

glycolytic rate (GR), which indicates the rate of lactate production versus glucose consumption, can also be estimated from m2 lactate × 2/m2 glucose. In the present experiments, the initial m2 glucose was 48.17%. Table 1A shows that lactate label distribution was not significantly altered when HT29 cells were treated with ECG at 70 or 140 μM.

ECG Treatment Reduced Glutamate Enrichment. The activity of the tricarboxylic acid (TCA) cycle was studied by glutamate mass isotopomer distribution analysis. Fluxes through the pyruvate dehydrogenase (PDH) and pyruvate carboxylase (PC) pathways were estimated from the levels of m2 isotopomers of C2−C4 and C2−C5 fragments (%PC = m2(C2−C4)/m2(C2−C5) and %PDH = (m2(C2−C5) − m2(C2−C4))/m2(C2−C5)), and ^{13}C glutamate enrichment was calculated as $\sum mn = m1 + m2 \times 2 + m3 \times 3$ for C2−C4 and C2−C5 glutamate fragments. Both 70 and 140 μM ECG-treated cells showed lower glutamate enrichment (Table 1B). The results also showed that whereas 140 μM ECG treatment increased the contribution of PC to the TCA cycle, it decreased glucose utilization through PDH (Figure 4).

ECG Inhibited Lipid Synthesis. Lipid synthesis is dependent on glucose carbons, as they are the primary source of acetyl-CoA, which is then incorporated into fatty acids through *de novo* synthesis. Acetyl-CoA enrichment was calculated from the m4/m2 ratio using the formula $m4/m2 = (n-1)/2 \times (q/1-q)$, where n is the number of acetyl units and q is the labeled fraction with p being the unlabeled fraction ($p + q = 1$). Therefore, to calculate the palmitate (C16)-labeled fraction, the formula is $(m4/m2)/3.5 = q/(1-q) = q/p$, whereas to calculate it for stearate (C18) we used $(m4/m2)/4 = q/(1-q) = q/p$. Next, we obtained the labeled fraction from $q = (q/p)/(1 + q/p)$. The contribution of glucose carbons to fatty acid synthesis was estimated by dividing the obtained q by the theoretical enrichment derived from glucose. Our results indicated that 140 μM ECG caused a 9% reduction in the contribution of glucose to both palmitate and stearate synthesis (Figure 5).

Lower *de Novo* Synthesis of RNA Ribose in ECG-Treated HT29 Cells. Table 1C shows the results of RNA ribose analysis. Whereas the ribose mass isotopomer m1 is formed when [1,2-$^{13}C_2$]-D-glucose is decarboxylated by the oxidative branch of the pentose phosphate pathway (PPP), the m2 mass isotopomer is synthesized by the reversible non-oxidative branch of the cycle. Therefore, the ratio of fluxes through oxidative and nonoxidative branches of the PPP can be estimated according to the formula ox:nonox = m1/m2 because the oxidative branch is necessary for m1 formation, whereas m2 species require the nonoxidative branch. The total ribose label incorporation is estimated as $\sum mn = m1 + m2 \times 2 + m3 \times 3 + m4 \times 4$. HT29 cells treated with 70 μM ECG did not show consistent differences in both ^{13}C enrichment and the ox:nonox ratio when compared to the control cells (Table 1C). On the contrary, treatment with 140 μM ECG decreased the ribose total ^{13}C enrichment in HT29 cells and significantly modulated the flux balance through the two branches of the PPP (ox:nonox ratio) in favor of the oxidative branch.

ECG Inhibited G6PD and TKT Specific Enzymatic Activities. The alteration in the balance between the fluxes through the oxidative and the nonoxidative branches of the PPP led us to examine the activity of the enzymes controlling this biosynthetic pathway, G6PD and TKT. The specific activities of these enzymes were compared between nontreated and ECG-treated cells (Figure 6). No significant changes in G6PD and TKT activities were detected in HT29 cells after treatment with 70 μM ECG. However, treatment with 140 μM ECG caused 15% reduction in G6PD and 35% reduction in TKT specific activities.

DISCUSSION

The characteristic metabolic adaptation underlying tumor progression represents the end point of several signaling cascades, but it also actively enhances the degree of tumor malignancy. In this framework, tumor metabolism represents a novel potential target to inhibit cancer cell growth. Because the grape and green tea catechin ECG has been linked to both tumor inhibition and modulation of metabolism, we examined the metabolic network of HT29 colon cancer cells in response to different concentrations of this polyphenol.

First, we determined the antiproliferative effect of ECG in HT29 cells. We showed that treatment with 70 μM ECG slightly affected HT29 cells. However, 140 μM ECG treatment for 72 h significantly induced S phase cell cycle arrest and apoptosis (Figure 2). Interestingly, the ECG concentrations selected for our study, 70 and 140 μM, can be reached physiologically in the intestinal lumen. In this regard,

Table 1. Mass Isotopomer Distribution[a]

A. Lactate Mass Isotopomer Distribution					
	m0	m1	m2	∑m*n*	GR (%)
control	0.7854 ± 0.0219	0.0203 ± 0.0050	0.1897 ± 0.0187	0.4134 ± 0.0423	77.9227 ± 7.7842
70 μM ECG	0.7927 ± 0.0095	0.01588 ± 0.0014	0.1891 ± 0.0110	0.4009 ± 0.0182	78.0257 ± 5.5051
140 μM ECG	0.7822 ± 0.01710	0.0269 ± 0.0093	0.1850 ± 0.01089	0.4144 ± 0.0283	75.3152 ± 4.7679

B. Glutamate Mass Isotopomer Distribution				
C2−C4	m0	m1	m2	∑m*n*
control	0.9573 ± 0.0195	0.0389 ± 0.0187	0.0026 ± 0.0016	0.0477 ± 0.0202
70 μM ECG	0.9763 ± 0.0141	0.0213 ± 0.0142 [a]	0.0011 ± 0.0006 [a]	0.0276 ± 0.0140 [a]
140 μM ECG	0.9834 ± 0.0044 [a]	0.0122 ± 0.0026 [ab]	0.0010 ± 0.0004 [a]	0.0240 ± 0.0139 [ab]

C2−C5	m0	m1	m2	∑m*n*
control	0.9486 ± 0.0081	0.0154 ± 0.0028	0.0339 ± 0.0049	0.0901 ± 0.0139
70 μM ECG	0.9659 ± 0.0046 [a]	0.0092 ± 0.0024 [a]	0.0241 ± 0.0023 [a]	0.0605 ± 0.0072 [a]
140 μM ECG	0.9861 ± 0.0026 [ab]	0.0043 ± 0.0012 [ab]	0.0075 ± 0.0013 [ab]	0.0243 ± 0.0043 [ab]

C. Ribose Mass Isotopomer Distribution							
	m0	m1	m2	m3	m4	∑m*n*	ox:nonox
control	0.5521 ± 0.0672	0.2597 ± 0.0443	0.1288 ± 0.0186	0.0438 ± 0.0122	0.01558 ± 0.0040	0.7109 ± 0.1107	2.0163 ± 0.3205
70 μM ECG	0.5237 ± 0.0232	0.2736 ± 0.0125	0.1310 ± 0.0123	0.0513 ± 0.0050	0.0202 ± 0.0042	0.7743 ± 0.0387	2.0885 ± 0.2205
140 μM ECG	0.6666 ± 0.0432 [ab]	0.2015 ± 0.0372 [ab]	0.0940 ± 0.0197 [ab]	0.0283 ± 0.0075 [ab]	0.0095 ± 0.0024 [ab]	0.5124 ± 0.0481 [ab]	2.1436 ± 0.5741 [ab]

[a]Mass isotopomer distribution in lactate, glutamate, and ribose after 72 h treatment of HT29 cells nontreated or treated with 70 and 140 μM ECG. (A) Lactate mass isotopomer distribution, ^{13}C enrichment (∑m*n*), and glycolytic rate (GR). (B) Mass isotopomer distribution and ^{13}C enrichment (∑m*n*) in fragments C2−C4 and C2−C5 from glutamate. (C) Mass isotopomer distribution, ^{13}C enrichment (∑m*n*), and the oxidative:nonoxidative ratio in RNA ribose. Values are expressed as mean ± standard error of three independent experiments. [a]Significantly different; [b]Significantly different from 70 μM ECG.

dx.doi.org/10.1021/jf3052785 | J. Agric. Food Chem. 2013, 61, 4310−4317

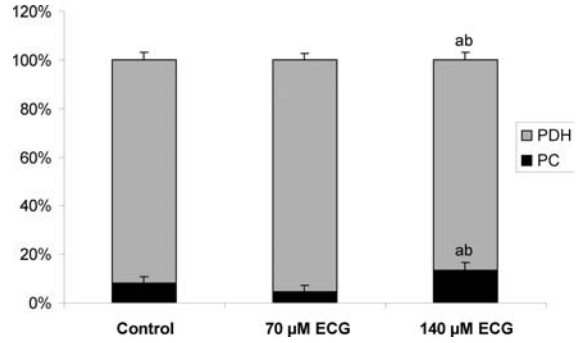

Figure 4. PC and PDH contributions to the TCA cycle were estimated using m2(C2−C4) and m2(C2−C5) − m2(C2−C4), respectively. Values are expressed as mean ± SD, $N = 3$. [a,b]Indicate a significant difference ($p < 0.05$) using Bonferroni multiple-comparison test following one-way ANOVA: [a]Significantly different from the control; [b]Significantly different from 70 μM ECG.

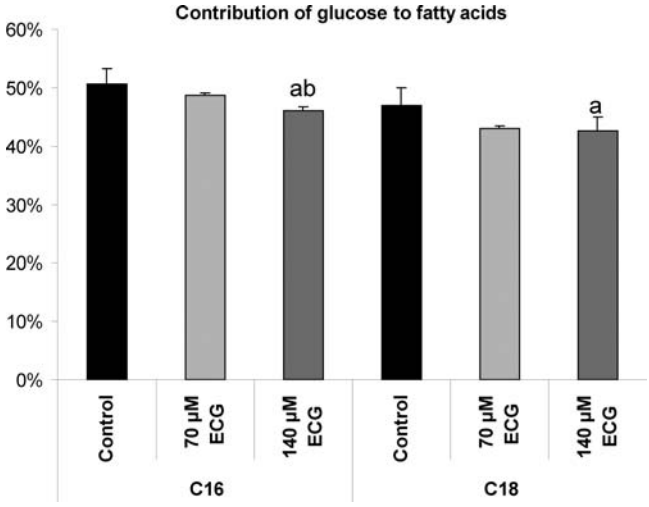

Figure 5. Determination of the relative contribution of glucose carbons to palmitate (C16) and stearate (C18) synthesis in ECG-treated cells and in control cells. Results are expressed as mean ± SD, $N = 2$. One-way ANOVA followed by Bonferroni test ($p < 0.05$): [a]Significantly different from control; [b]Significantly different from 70 μM ECG.

Vaidyanathan and Walle described that the concentration of ECG in the lumen may range between 75 and 300 μM after having a cup of tea and that ECG is extensively taken up by colonic cells.

Neoplastic cells increase glycolysis to produce anabolic precursors and energy.[14] To maintain this high rate of glycolysis, tumor cells must have access to an elevated supply of glucose. In this regard, our results showed that HT29 cells treated with 140 μM ECG exhibited a lower glucose uptake compared to HT29 control cells (Figure 3). This result is in agreement with the reported antidiabetic and antiobesity properties of green tea, which have been related to the regulation of gene expression associated with glucose uptake.[15] However, ECG treatment did not affect the product of anaerobic glycolysis, the lactate, neither in biochemical analysis nor in mass isotopomer distribution analysis. Moreover, the estimated glycolytic flux (GR) did not show modifications after ECG treatment. This estimated GR indicated that in all cases 75−78% of the lactate was derived directly from glucose. Consistently, our glycolytic rate measurements in HT29 cells

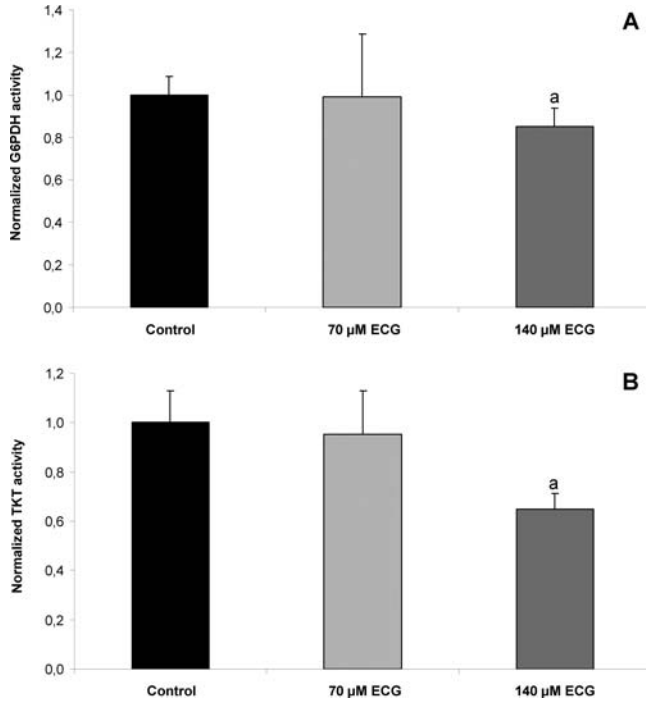

Figure 6. Plot of fold changes in G6PD (A) and TKT (B) activities in ECG-treated versus nontreated HT29 cells. Results show the mean ± SD, $N = 4$. $p < 0.01$ (**) versus untreated cells. Data were analyzed using the Bonferroni test after one-way ANOVA: [a]Significantly ($p < 0.05$) different from control.

were in agreement with those previously reported by Alcarraz-Vizán et al.[16] In this regard, taking into account the determined GR, lactate production was greater than that expected from glucose consumption alone, indicating that lactate was produced from additional carbon sources such as pyruvate, glutamine, and amino acids.

Regarding glutamate mass isotopomer analysis in fragments C2−C4 and C2−C5, we observed a reduction in ^{13}C enrichment in all the fractions of glutamate after ECG treatments (Table 1B). This result may be explained by the reduced glucose uptake and the consequent decrease in ^{13}C entrance in the Krebs cycle. Moreover, given that there is no change in lactate production, we definitely conclude that it has to be produced from other metabolites such as glutamine, which showed an increase in consumption after 140 μM ECG treatment (Figure 3) probably to compensate the considerable decrease in glucose consumption. However, whereas 140 μM ECG treatment reduced glucose consumption by 77%, it increased glutamine consumption only by 48%, producing a lack of metabolic precursors and energy. Furthermore, the analysis of glutamate fragments allowed us to calculate the contributions of PC and PDH to the TCA cycle (Figure 4). ^{13}C from [1,2-$^{13}C_2$]-D-glucose can enter into mitochondrial citrate by the action of PDH or via the anaplerotic carboxylation of pyruvate catalyzed by PC. Then, transamination of α-ketoglutarate produces labeled glutamate that is excreted in the media. Depending on the pathway mediating entry into the mitochondria, a different labeling pattern is obtained in C2−C4 and C2−C5 glutamate fragments. In HT29 cells, both PDH and PC entry points were active, although the PDH flux was more significant (around 90%) (Figure 4). Interestingly, 140 μM ECG produced a disequilibrium in glucose utilization

dx.doi.org/10.1021/jf3052785 | J. Agric. Food Chem. 2013, 61, 4310−4317

through these routes, enhancing the contribution of the PC flux and reducing the characteristic high tumor flux through PDH.

Moreover, we determined label incorporation into the fatty acids palmitate (C16) and stearate (C18) and calculated the contribution of glucose to lipid synthesis (Figure 5). Our results showed lower lipogenic activity in ECG-treated cells, which could be related to the inhibition of the synthesis of essential components of cellular membranes required for accelerated proliferation in HT29 cells.

Finally, the analysis of ribose shown in Table 1C demonstrated that low ECG concentration did not cause significant changes in its mass isotopomer distribution. Noteworthy, mass isotopomer distribution analysis experiments were performed at 72 h, when metabolic enrichment of ^{13}C from [1,2-$^{13}C_2$]-D-glucose is almost saturated in this condition. However, the metabolic enrichment of ^{13}C in high ECG concentration was lower and not saturated, indicating that there was less *de novo* synthesis of ribose in this condition. This lower ribose synthesis is associated with the high inhibition of cancer cell growth produced by 140 μM ECG treatment (Figure 1B). It is worth noting that PPP inhibition in different tumor cell lines decreases tumor cell proliferation.[22,23] Furthermore, inhibition of nucleic acid synthesis has been shown to be a successful chemotherapy strategy.[24] Ribose can be synthesized from the glycolytic intermediate glucose 6-phosphate via the oxidative branch of the PPP as well as from fructose 6-phosphate and glyceraldehyde 3-phosphate via the nonoxidative branch of the PPP. Mass isotopomer distribution analysis in ribose showed a significant increase in the ox:nonox ratio after treatment with high concentrations of ECG. These findings prompted us to further analyze PPP activity after ECG treatment. Examination of the activities of the key enzymes in the PPP, G6PD, and TKT showed that both enzymatic activities were reduced in 140 μM ECG-treated cells (Figure 6). Moreover, in agreement with the reported increase in the ox:nonox ratio, the inhibition of TKT was more important than the reduction in G6PD. Given that the control coefficients on tumor cell growth for G6PD and TKT have been reported to be 0.41 and 0.9, respectively,[25] the 35% reduction in TKT activity induced by ECG may indicate an important inhibition of nucleic acid synthesis and tumor growth. Interestingly, in several tumor-derived cell lines, the nonoxidative branch of the PPP is the main source for ribose-5-phosphate synthesis,[26] which underscores the importance of this inhibition. Although to a lesser extent, G6PD activity was also inhibited (15%), which could be biologically important because the oxidative branch of the PPP not only enables cells to synthesize more ribose for nucleic acid requirements but also mediates the recruitment of reducing power in the form of NADPH necessary for membrane lipid synthesis.

It has been reported that the pattern of metabolic changes is associated with the type of cell death and growth inhibition involved in the cytotoxic action of a determined drug.[27] Moreover, the precise metabolic phenotype of cancer cells has been reported to be dependent on cell type and growth conditions[28] even in the microregions of the same tumor.[29] In our study, ECG acted mainly by reducing the synthesis of macromolecules needed to produce a new cell, hence inhibiting colon cancer cell growth. In future studies, it would be interesting to determine whether these metabolic changes induced by ECG are common to other colon cancer models.

In summary, incubation with different concentrations of ECG modified the metabolic profile in HT29 cells by targeting the incorporation of nutrients into the biomass. ECG reduced glucose uptake and inhibited the anabolic pathways required to satisfy the metabolic requirements associated with increased tumor proliferation. Our results indicate that bioactive compounds such as polyphenols may play a role in cancer therapy as nutritional supplements by controlling tumor viability through the regulation of glucose carbon redistribution.

AUTHOR INFORMATION

Corresponding Author

*Phone: 0034 934021593. Fax: 0034 934021559. E-mail: martacascante@ub.edu.

Present Address

$^{\perp}$(G.A.-V.) Diabetes and Obesity Laboratory, Institut d'Investigacions Biomèdiques August Pi i Sunyer (IDIBAPS), Centre Esther Koplowitz (CEK), Rosselló 149-153, 08036 Barcelona, Spain.

Funding

Financial support was provided by grants SAF2008-00164, SAF2011-25726, AGL2006-12210-C03-02/ALI, and AGL2009-12374-C03-03/ALI from the Spanish government Ministerio de Economía y Competitividad and personal financial support (FPU program) and from the Red Temática de Investigación Cooperativa en Cáncer, Instituto de Salud Carlos III, Spanish Ministry of Science and Innovation & European Regional Development Fund (ERDF) "Una manera de hacer Europa" (ISCIII-RTICC grants RD06/0020/0046). We have also received financial support from the AGAUR-Generalitat de Catalunya (grant 2009SGR1308, 2009 CTP 00026, and Icrea Academia Award 2010 granted to M.C.) and the European Commission (FP7) ETHERPATHS KBBE-grant agreement no. 22263.

Notes

The authors declare no competing financial interest.

ACKNOWLEDGMENTS

The authors thank Dr. Pedro Vizán for helpful advice.

REFERENCES

(1) Jemal, A.; Center, M. M.; DeSantis, C.; Ward, E. M. Global patterns of cancer incidence and mortality rates and trends. *Cancer Epidemiol. Biomarkers Prev.* **2010**, *19* (8), 1893−1907.

(2) Ramos, S.; Rodriguez-Ramiro, I.; Martin, M. A.; Goya, L.; Bravo, L. Dietary flavanols exert different effects on antioxidant defenses and apoptosis/proliferation in Caco-2 and SW480 colon cancer cells. *Toxicol. in Vitro* **2011**, *25* (8), 1771−1781.

(3) Baek, S. J.; Kim, J. S.; Jackson, F. R.; Eling, T. E.; McEntee, M. F.; Lee, S. H. Epicatechin gallate-induced expression of NAG-1 is associated with growth inhibition and apoptosis in colon cancer cells. *Carcinogenesis* **2004**, *25* (12), 2425−2432.

(4) Chen, Y. K.; Cheung, C.; Reuhl, K. R.; Liu, A. B.; Lee, M. J.; Lu, Y. P.; Yang, C. S. Effects of green tea polyphenol (−)-epigallocatechin-3-gallate on newly developed high-fat/Western-style diet-induced obesity and metabolic syndrome in mice. *J. Agric. Food Chem.* **2012**, *59* (21), 11862−11871.

(5) Shimizu, M.; Kubota, M.; Tanaka, T.; Moriwaki, H. Nutraceutical approach for preventing obesity-related colorectal and liver carcinogenesis. *Int. J. Mol. Sci.* **2012**, *13* (1), 579−595.

(6) Dang, C. V.; Hamaker, M.; Sun, P.; Le, A.; Gao, P. Therapeutic targeting of cancer cell metabolism. *J. Mol. Med. (Berlin, Ger.)* **2011**, *89* (3), 205−212.

(7) Vizan, P.; Sanchez-Tena, S.; Alcarraz-Vizan, G.; Soler, M.; Messeguer, R.; Pujol, M. D.; Paul Lee, W. N.; Cascante, M. Characterization of the metabolic changes underlying growth factor

angiogenic activation: identification of new potential therapeutic targets. *Carcinogenesis* **2009**, *30* (6), 946−952.
(8) Vizan, P.; Boros, L. G.; Figueras, A.; Capella, G.; Mangues, R.; Bassilian, S.; Lim, S.; Lee, W. N.; Cascante, M. K-ras codon-specific mutations produce distinctive metabolic phenotypes in NIH3T3 mice [corrected] fibroblasts. *Cancer Res.* **2005**, *65* (13), 5512−5515.
(9) Sanchez-Tena, S.; Fernandez-Cachon, M. L.; Carreras, A.; Mateos-Martin, M. L.; Costoya, N.; Moyer, M. P.; Nunez, M. J.; Torres, J. L.; Cascante, M. Hamamelitannin from witch hazel (*Hamamelis virginiana*) displays specific cytotoxic activity against colon cancer cells. *J. Nat. Prod.* **2012**, *75* (1), 26−33.
(10) Liu, T.; Zhu, W.; Yang, X.; Chen, L.; Yang, R.; Hua, Z.; Li, G. Detection of Apoptosis Based on the Interaction between annexin V and phosphatidylserine. *Anal. Chem.* **2009**, *81* (6), 2410−2413.
(11) Lee, W. N.; Boros, L. G.; Puigjaner, J.; Bassilian, S.; Lim, S.; Cascante, M. Mass isotopomer study of the nonoxidative pathways of the pentose cycle with [1,2-$^{13}C_2$]glucose. *Am. J. Physiol.* **1998**, *274* (5 Pt 1), E843−E851.
(12) Boren, J.; Lee, W. N.; Bassilian, S.; Centelles, J. J.; Lim, S.; Ahmed, S.; Boros, L. G.; Cascante, M. The stable isotope-based dynamic metabolic profile of butyrate-induced HT29 cell differentiation. *J. Biol. Chem.* **2003**, *278* (31), 28395−28402.
(13) Boren, J.; Cascante, M.; Marin, S.; Comin-Anduix, B.; Centelles, J. J.; Lim, S.; Bassilian, S.; Ahmed, S.; Lee, W. N.; Boros, L. G. Gleevec (STI571) influences metabolic enzyme activities and glucose carbon flow toward nucleic acid and fatty acid synthesis in myeloid tumor cells. *J. Biol. Chem.* **2001**, *276* (41), 37747−37753.
(14) Vander Heiden, M. G.; Cantley, L. C.; Thompson, C. B. Understanding the Warburg effect: the metabolic requirements of cell proliferation. *Science* **2009**, *324* (5930), 1029−1033.
(15) Cao, H.; Hininger-Favier, I.; Kelly, M. A.; Benaraba, R.; Dawson, H. D.; Coves, S.; Roussel, A. M.; Anderson, R. A. Green tea polyphenol extract regulates the expression of genes involved in glucose uptake and insulin signaling in rats fed a high fructose diet. *J. Agric. Food Chem.* **2007**, *55* (15), 6372−6378.
(16) Alcarraz-Vizan, G.; Boren, J.; Lee, W. N.; Cascante, M. Histone deacetylase inhibition results in a common metabolic profile associated with HT29 differentiation. *Metabolomics* **2010**, *6* (2), 229−237.
(17) Amoedo, N. D.; Rodrigues, M. F.; Pezzuto, P.; Galina, A.; da Costa, R. M.; de Almeida, F. C.; El-Bacha, T.; Rumjanek, F. D. Energy metabolism in H460 lung cancer cells: effects of histone deacetylase inhibitors. *PLoS One* **2011**, *6* (7), e22264.
(18) Le, A.; Lane, A. N.; Hamaker, M.; Bose, S.; Gouw, A.; Barbi, J.; Tsukamoto, T.; Rojas, C. J.; Slusher, B. S.; Zhang, H.; Zimmerman, L. J.; Liebler, D. C.; Slebos, R. J.; Lorkiewicz, P. K.; Higashi, R. M.; Fan, T. W.; Dang, C. V. Glucose-independent glutamine metabolism via TCA cycling for proliferation and survival in B cells. *Cell Metab.* **2012**, *15* (1), 110−121.
(19) Weinberg, F.; Hamanaka, R.; Wheaton, W. W.; Weinberg, S.; Joseph, J.; Lopez, M.; Kalyanaraman, B.; Mutlu, G. M.; Budinger, G. R.; Chandel, N. S. Mitochondrial metabolism and ROS generation are essential for Kras-mediated tumorigenicity. *Proc. Natl. Acad. Sci. U.S.A.* **2010**, *107* (19), 8788−8793.
(20) Chen, E. I.; Hewel, J.; Krueger, J. S.; Tiraby, C.; Weber, M. R.; Kralli, A.; Becker, K.; Yates, J. R., 3rd; Felding-Habermann, B. Adaptation of energy metabolism in breast cancer brain metastases. *Cancer Res.* **2007**, *67* (4), 1472−1486.
(21) Sun, R. C.; Board, P. G.; Blackburn, A. C. Targeting metabolism with arsenic trioxide and dichloroacetate in breast cancer cells. *Mol. Cancer* **2011**, *10*, 142.
(22) Cascante, M.; Boros, L. G.; Comin-Anduix, B.; de Atauri, P.; Centelles, J. J.; Lee, P. W. Metabolic control analysis in drug discovery and disease. *Nat. Biotechnol.* **2002**, *20* (3), 243−249.
(23) Comin-Anduix, B.; Boren, J.; Martinez, S.; Moro, C.; Centelles, J. J.; Trebukhina, R.; Petushok, N.; Lee, W. N.; Boros, L. G.; Cascante, M. The effect of thiamine supplementation on tumour proliferation. A metabolic control analysis study. *Eur. J. Biochem.* **2001**, *268* (15), 4177−4182.
(24) Purcell, W. T.; Ettinger, D. S. Novel antifolate drugs. *Curr. Oncol. Rep.* **2003**, *5* (2), 114−125.
(25) Boren, J.; Montoya, A. R.; de Atauri, P.; Comin-Anduix, B.; Cortes, A.; Centelles, J. J.; Frederiks, W. M.; Van Noorden, C. J.; Cascante, M. Metabolic control analysis aimed at the ribose synthesis pathways of tumor cells: a new strategy for antitumor drug development. *Mol. Biol. Rep.* **2002**, *29* (1−2), 7−12.
(26) Cascante, M.; Centelles, J. J.; Veech, R. L.; Lee, W. N.; Boros, L. G. Role of thiamin (vitamin B-1) and transketolase in tumor cell proliferation. *Nutr. Cancer* **2000**, *36* (2), 150−154.
(27) Motrescu, E. R.; Otto, A. M.; Brischwein, M.; Zahler, S.; Wolf, B. Dynamic analysis of metabolic effects of chloroacetaldehyde and cytochalasin B on tumor cells using bioelectronic sensor chips. *J. Cancer Res. Clin. Oncol.* **2005**, *131* (10), 683−691.
(28) Telang, S.; Lane, A. N.; Nelson, K. K.; Arumugam, S.; Chesney, J. The oncoprotein H-RasV12 increases mitochondrial metabolism. *Mol. Cancer* **2007**, *6*, 77.
(29) dos Santos, M. A.; Borges, J. B.; de Almeida, D. C.; Curi, R. Metabolism of the microregions of human breast cancer. *Cancer Lett.* **2004**, *216* (2), 243−248.